ACS OMEGA

http://pubs.acs.org/journal/acsodf

Article

Acoustic Attenuation and Dispersion in Fatty Tissues and Tissue Phantoms Influencing Ultrasound Biomedical Imaging

Teng Yang, Yuqi Jin, and Arup Neogi*

Cite This: *ACS Omega* 2023, 8, 1319−1330

Read Online

ACCESS | Metrics & More | Article Recommendations

ABSTRACT: The development of ultrasonic imaging techniques is optimized using artificial tissue phantoms before the practical applications. However, due to the strong attenuation and dispersion, accumulated fatty tissues can significantly impact the resolution and even feasibility of certain ultrasonic imaging modalities. An appropriate characterization of the acoustic properties on fatty phantoms can help the community to overcome the limitations. Some of the existing methods heavily overestimate attenuation coefficients by including the reflection loss and dispersion effects. Hence, in this study, we use numerical simulation-based comparison between two major attenuation measurement configurations. We further pointed out the pulse dispersion in viscoelastic tissue phantoms by simulations, which barely attracted attention in the existing studies. Using the selected attenuation and dispersion testing methods that were selected from the numerical simulation, we experimentally characterized the acoustic properties of common fatty tissue phantoms and compared the acoustic properties with the natural porcine fatty tissue samples. Furthermore, we selected one of the tissue phantoms to construct ultrasound imaging samples with some biomasses. With the known attenuation and dispersion of the tissue phantom, we showed the clarity enhancement of ultrasound imaging by signal post-processing to weaken the attenuation and dispersion effects.

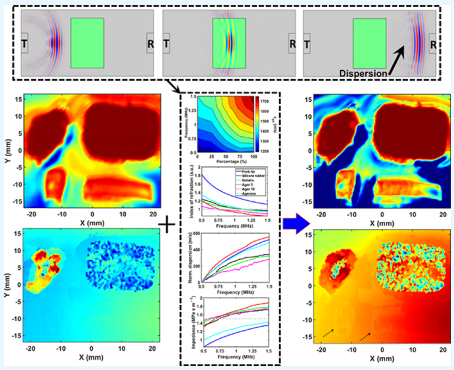

1. INTRODUCTION

In the human body, soft tissues, like fat, muscle, ligaments, and tendons, connect and provide support and protection for structures and organs.[1] Most tissue phantom research focuses on mimicking the mechanical, acoustic, and biomedical properties since natural tissues are expensive, inconsistent, and hard to preserve.[2] One of the major obstacles to ultrasound diagnostic in a clinic setting is the high dispersion and dissipation of the soft tissues in heavy body fluids or high body mass index environments.[3−5] The studies of the acoustic properties of tissue phantoms can pave the way to further the development of medical imaging techniques and their practical applications by accurately representing the actual human tissues. Many approaches were mentioned in the existing literature to improve ultrasound resolution. Vogt et al. have demonstrated high-resolution ultrasound imaging methods and the practical performance using high frequency photoacoustic imaging.[6,7] Recent attempts have been directed toward applying machine learning techniques to medical images to enhance accuracy in diagnosis.[8−10] AI-assisted diagnosis is possible with well-understood tissue phantoms for generating an AI training bank without using a massive quantity of natural human tissues, which has considerable uncertainties.[11] However, the acoustic properties of the tissue phantom and the natural tissues need to be studied thoroughly and associated with their elastic properties and, more importantly, correctly distinguished to attain this objective.

Among all the acoustic properties, speed of sound, impedance, attenuation, back-scattering coefficient, and nonlinearity parameters have been extensively studied.[12−15] One of the significant characteristics of acoustic waves, dispersion, is rarely discussed or considered in prior works, although dispersion critically influences the temporal resolution in ultrasound imaging. This study examined the acoustic properties, especially the dispersion coefficient of four widely used soft tissue-mimicking materials: gelatin, agar, silicone rubber, and agarose, using the proposed technique. Gelatin gels and agar gels are the earliest soft tissue-mimicking material for ultrasound imaging due to their closeness to soft tissue mechanical and acoustic properties, relatively low cost, and convenience.[5,16] Agarose is a natural polysaccharide polymer with unique biocompatibility, thermoreversible gelation behavior, and physiochemical feature used for tissue engineer-

Received: October 20, 2022
Accepted: December 13, 2022
Published: December 21, 2022

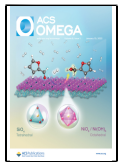

ACS Publications

© 2022 The Authors. Published by American Chemical Society

ing applications.[17,18] Silicone rubber-based gels are mainly for skeletal muscle[19] and breast-related research.[20,21] Moreover, researchers mix other ingredients into those gels to tune the acoustic properties. This study will also investigate the acoustic changes induced by adding evaporated milk into gelatin[22] or mineral oil into silicone rubber[23] at different concentrations.

The acoustic attenuation is generally considered the primary factor affecting the ultrasound imaging clarity due to the characteristic acoustic properties of the tissue phantoms. However, in principle, the attenuation can only reduce the signal-to-noise ratio of the collected signal, which is not directly affecting imaging clarity. However, the dispersion of the acoustic waves due to the medium's elastic properties can lead to a temporal pulse broadening, resulting in a lower temporal resolution to yield an inferior image quality. The dispersive properties of the biomaterial will help tailor tissue-mimicking phantoms for ultrasound-based diagnostics. It will be especially useful for developing elastography since tissue-mimicking phantoms with well-defined acoustic properties, dimensions, and internal structures are necessary for calibrating and characterizing ultrasound imaging systems. Furthermore, materials with tunable ultrasound properties are essential for biological tissue replacements, medical devices, ultrasound diagnostic, and drug delivery systems.[24]

Acoustic properties such as the group velocity dispersion, attenuation, and frequency-dependent dispersion within conventionally used soft-tissue phantoms have been studied. Most prior work on the ultrasonic characterization of the biomaterial is limited to estimating acoustic attenuation of tissue phantoms. However, the attenuation coefficients are generally overestimated due to the contribution from reflection and dispersion within the tissue medium. In this study, we performed numerical simulations to present the performance and suitability of the conventional bistatic immersion test for acoustic attenuation measurement. The performance was then compared with the monostatic in-air test method developed in this work using the experimental setup shown in Figure 1. The acoustic properties of the tissue phantoms were compared with natural porcine samples with an excess of fatty tissue.

2. MATERIALS AND EXPERIMENTAL METHODS

2.1. Density Calculation. To compare the density of tissue phantoms with natural tissues and calculate the acoustic properties, we used the traditional weight divided by volume methods to calculate the density of tissue phantoms. A precision balance 440-47N from KERN with a resolution of 0.1 g was used for measuring the weight. A 6 in stainless steel vernier caliper was used to measure the dimensions of the tissue phantom with an accuracy of 0.02 mm. The density ρ of the samples was calculated via $\rho = m/v$.

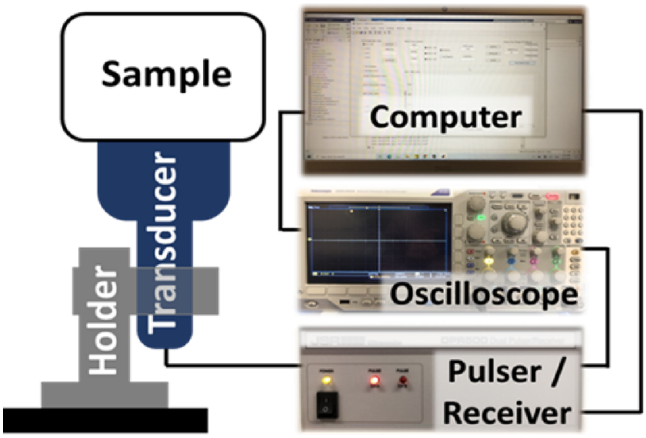

Figure 1. Monostatic experimental setup for the acoustic property's measurements.

2.2. Numerical Simulation. In this study, all the numerical simulations were performed by finite element analysis (FEA)-based numerical simulation software: COMSOL Multiphysics. The pulse waveform in the simulation was expressed as $x(t) = \sin(2\pi f_0 t)e^{-f_0(t-\delta T_0)^2}$, where f_0, T_0, and δ were the fundamental frequency, period, and delay of the pulse, respectively. All the temporal domain numerical simulation models were studied in a time range from 0 to $100T_0$ with $0.2T_0$ intervals. The numerical simulation cases can be grouped into two cases, bistatic transmission tests and monostatic time-of-flight tests. The samples were placed in a water ambient domain in the bistatic simulation. The acoustic emission source and boundary detection probe were located on two sides of the water ambient domain. The distance between sample surfaces and source/probe was larger than the operating wavelength following the practical experimental setup from some literature. The outer boundary of the water ambient domain was set to impedance boundary conditions with the acoustic impedance value of water, which can represent a large enough water tank in a practical case to eliminate the reflection from the water tank walls. In monostatic instances, the samples were apart from the acoustic emission source with a thin layer of coupling material. We used a 1 mm-thick water layer as the selected coupling material with a much smaller operating wavelength. The outer boundary of the sample in the monostatic simulation was set up to sound hard boundary that refers to a reflection boundary condition to eliminate the energy radiation, which was comparable to the practical sample/air impedance mismatch conditions in the experiments. The tissue phantom sample in the numerical simulation was set with speed of sound and density values of 1600 m/s and 1200 kg m^{-3}, respectively.

2.3. Experimental Setups. For measurement, a JSR 500 pulse/receiver and Tek 3024b 2.5GHz oscilloscope were used to generate and acquire data. Olympus 1 MHz 1″ V302 transducers were used in a monostatic setup. The dispersion and attenuation in a monostatic (pulse-echo) arrangement required gain on the pulse-echo, resulting in significant signal distortion. The selection of the bistatic arrangement decreased experimental error induced by dispersion, attenuation, and gain on detected ultrasound. Pulses were measured at 22.4 °C (room temperature). The sound propagation speed in the samples using standard time-of-flight techniques was calculated from the ratio of specimen thickness to sound wave transit time. The accuracy of the setup was verified for DI water.

2.4. Biomaterials Materials. *2.4.1. Gelatin with Evaporated Milk.* The gelatin phantoms were made with Knox unflavored gelatin powder, ranging around 200−225 blooms defined by the manufacturer. Evaporated milk (Nestlé Carnation Evaporated Milk: Vitamin D added) containing 6.3% fat was used to replace the water to increase the speed of sound and attenuation of the final product.[25] We used weight percent to calculate the percentage of evaporated milk and gelatin powder. A precision balance 440-47N from KERN with a resolution of 0.1 g was used for measuring the weight. For

https://doi.org/10.1021/acsomega.2c06750
ACS Omega 2023, 8, 1319−1330

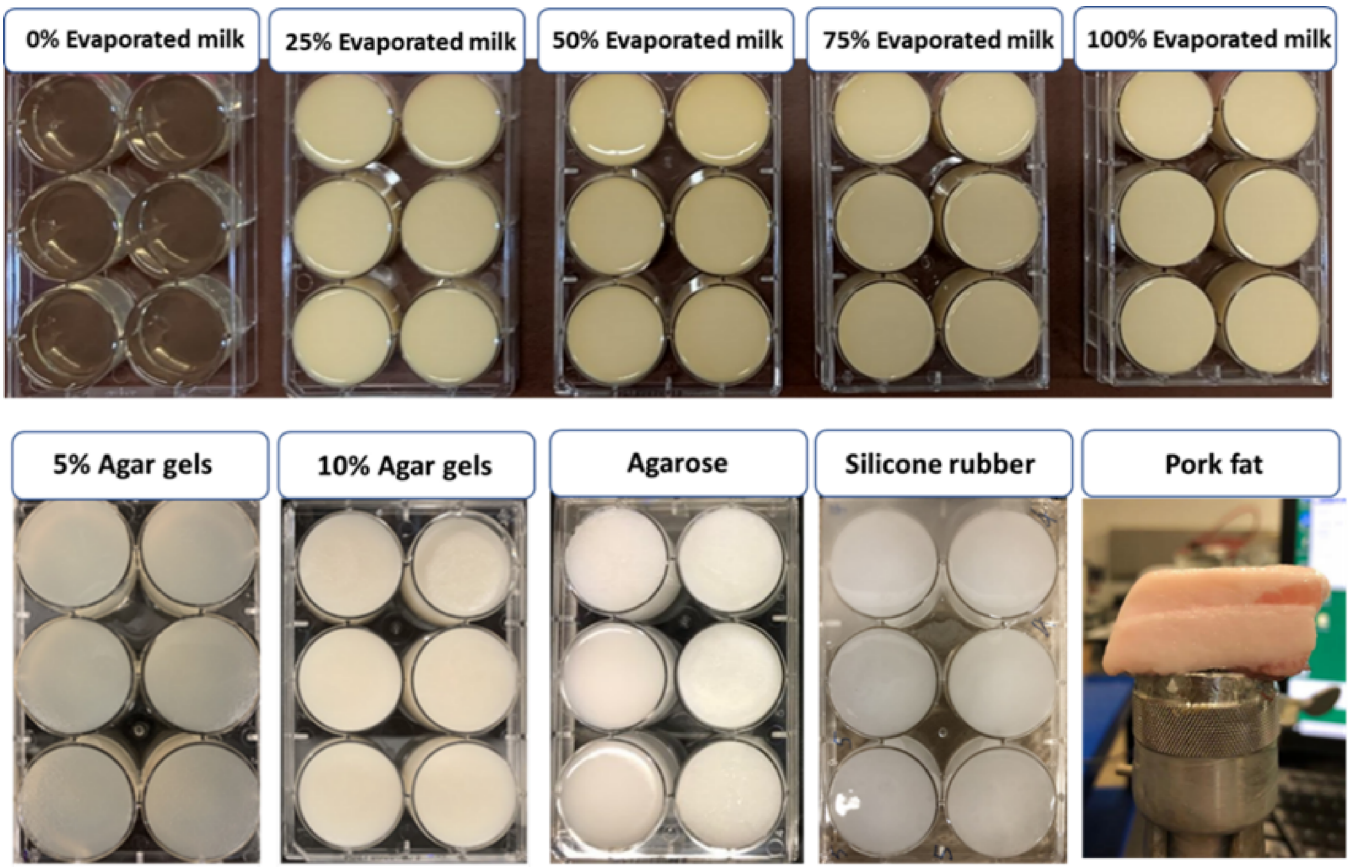

Figure 2. Photographs of the tissue phantom samples and one of the fatty pork samples.

example, in Figure 2, 0% evaporated milk means plain 10 wt % gelatin phantom. Evaporated milk (25%) means 25 g of evaporated milk and 75 g of deionized and degassed water with 10 g of gelatin powder. Evaporated milk (50%) means 50 g of evaporated milk and 50 g of deionized and degassed water with 10 g of gelatin powder. For 0% evaporated milk gelatin gels, we poured 100 g of deionized and degassed water in a sanitized 800 mL PYREX beaker. A Corning PC 420 hot plate stirrer with a temperature range from 25 to 500 °C and stirrer speed from 60 to 1100 RPM was used to mix and heat the mixture of evaporated milk and water. We first heated the water to boiling temperature, then put the gelatin power, and thoroughly stirred until all the powder was fully dissolved. We poured the 80 °C evaporated milk into the mixture and stirred until a uniform liquid was formed. This mixture was cooled at room temperature to 40 °C before pouring into a greiner bio-one CELLSTAR cell culture six-well plate with 550 × 300 × 245 mm for molding. We measured the acoustic properties of the gels after 24 h of curing time under room temperature.

2.4.2. Agar Tissue Phantoms. Agar is a polysaccharide vegetarian substitute for gelatin extracted from red algae, such as Gracilaria and Gelidium. Agar powder, 100% nature seaweed by ECO-TASTE, was used to make agar gels with 5 and 10 wt % concentrations. For 5 wt % agar gels, 5 g of agar powder was dissolved in 100 g of deionized and degassed water, and the mixture was heated up to the boiling point and kept for 2 min with constant stirring.[18] The mixture was then cooled down at room temperature for 24 h. We used the same six-well plates to mold the agar gel phantom. The 10 wt % agar gel follows the same procedure. We used 10 g of agar powder and 100 g of water.

2.4.3. Agarose Tissue Phantoms. Agarose is a linear polymer of agarobiose, a disaccharide made from D-galactose and 3,6-anhydro-L-galactopyranose.[26] Agarose was purified from agar or extracted from red seaweed.

The agarose tissue phantoms were used to mimic fatty tissue phantoms according to the study of Ortega et al.[27] The ingredient includes agarose (0.6 g), tri-distilled water (20 mL), neutral detergent (4 mL), and mineral oil (20 mL). In our research, we selected agarose powder A1700 from Benchmark Scientific. The procedure was as follows:

1. Measuring the quantification of the materials.
2. Mixing the tri-distilled water with neutral detergent and stirring until obtaining a homogeneous solution.
3. Adding the mineral oil to the mixture.
4. Heating the mixture to 65 °C.
5. Adding agarose powder and stirring well.
6. Pouring into a six-well cell culture plate same as before and cooling under room temperature.

2.4.4. Silicone Rubber with Mineral Oil. Silicone rubber phantoms are generally used to mimic realistic-shaped human phantoms due to their flexibility and durability.[28] Unlike gelatin, agar, or agarose biopolymers that contain over 80% of water and have a stiffness similar to soft tissues, silicon-based phantoms have a wide range of mechanical properties that can provide additional advantages and wide applications, such as tumor mimicking, breast mimicking, and needle insertion simulation.[23] Since silicone rubber does not contain water, they do not suffer from evaporation or bacterial growth, making them a good candidate for combining with other materials such as nanoparticles, glycerin, and oil to provide a

https://doi.org/10.1021/acsomega.2c06750
ACS Omega 2023, 8, 1319−1330

variety of optical properties.[29] In this study, we used OOMOO 30 Tin-Cure silicone rubber from SMOOTH-ON to make tissue phantoms and doped it with different percentages of mineral oil to tune the acoustic properties. The procedure follows the manufacturer's instructions.

We first measured equal amounts of liquid parts A and B, mixed liquid A with the corresponding percentage of mineral oil, then combined with liquid B, stirring the mixture until rubber contents were mixed thoroughly, then poured over the prepared six-well model, and let it cure to a solid, flexible rubber mold.

All the gelatin and silicone rubber samples were performed with the degassing process. In the case of agar and agarose samples, the samples were separated into two cartographies specifically with and without degassing processing.

3. THEORY

3.1. Attenuation Measurement. A very simple mono-static experimental setup was used for the attenuation measurement through the biomaterials, as shown in Figure 1. In the acoustic attenuation measurements, we separated the work into two parts. The property was determined in the temporal domain and frequency domain. As the conventional method described, the amplitude reduction of the pulse through the tested sample was estimated as group attenuation. The effect is contributed by the energy dissipation of all the frequency components in the pulse envelope and the out-of-phase effect between the frequency components. The values were calculated by the expression

$$A = -20\log_{10}\left(\frac{p_2}{p_1}\right)d^{-1} \tag{1}$$

where A is the attenuation coefficient, p_2 and p_1 are the maximum points of the pulse amplitude of the first and second roundtrip reflections, and d is the twice sample thickness along the wave propagation direction.

In addition, to separate between the dispersion effect-induced amplitude decreasing on the pulse envelope and the energy dissipation on the frequency components, we have translated the collected pulse envelope into the frequency domain to find the magnitude drop of each frequency component, which described accurate attenuation. In this work, we notated it as frequency-dependent attenuation, as the following expression shows

$$A(f) = -20\log_{10}\left(\frac{p_2(f)}{p_1(f)}\right)d^{-1} \tag{2}$$

where $A(f)$, $p_2(f)$, and $p_1(f)$ are the frequency-dependent variables.

3.2. Frequency-Dependent Speed of Sound from Time Domain Sound Wave Propagation. We aim to estimate the frequency-dependent speed of sound from the time-dependent signal as measured in the sample compared to that in water. The linear response theory is applied to calculate the frequency-dependent speed of sound.

We start with the equation[19]

$$c_{\text{sample}}(f) = \frac{c_{\text{water}}(f)}{1 + \frac{c_{\text{water}}(f)\Delta t(f)}{d_{\text{sample}}}} \tag{3}$$

where c_{sample} is the speed of sound for the sample, $\Delta t(f)$ is the time delay at a given frequency relative to water, c_{water} is the speed of sound of water, and d_{sample} is the sample thickness. For dispersive media, Δt and c_{sample} are frequency-dependent functions, whereas c_{water} remains constant since the water is non-dispersive media.

A time-dependent pulse is characterized by its frequency-dependent Fourier transform. To determine $\Delta t(f)$from the time domain data, the causality principle is used to describe the recorded wave signal in a linear system,[30]$y(t)$, as

$$y(t) = \int_{-\infty}^{t} s(t - t')\cdot r(t')\mathrm{d}t' \tag{4}$$

where $s(t)$ is the impulse response of the sample material and $r(t)$ is the reference signal from pure water. Applying the convolution theorem to eq 4, we get a linear relation for the Fourier transforms

$$Y(f) = S(f)\cdot R(f) = x(f)\cdot e^{i\alpha(f)}\cdot y(f)\cdot e^{i\beta(f)} \tag{5}$$

Here, $S(f)$ and $R(f)$ are the Fourier transforms of the signal from sample and water, respectively.$\alpha(f)$and $\beta(f)$ refer to the phase of the waveforms, and $x(f)$ and $y(f)$ represent the frequency-dependent amplitude of the Fourier spectra.

The response function $S(f)$ can also be written in a standard complex form, frequency-dependent representing exponential decay[19]

$$S(f) = e^{-i2\pi\Delta t(f)}\cdot e^{-\alpha(f)d_{\text{sample}}} \tag{6}$$

The time delay at a given frequency of sample as compared to pure water[31] is

$$\Delta t(f) = \frac{\alpha - \beta}{2\pi f} \tag{7}$$

Substitution of eq 7 into eq 3 results in the final frequency-dependent speed of sound

$$c_{\text{sample}}(f) = \frac{d_{\text{sample}}}{\frac{d_{\text{sample}}}{c_{\text{water}}} + \frac{\alpha(f) - \beta(f)}{2\pi f}} \tag{8}$$

4. RESULTS AND DISCUSSIONS

4.1. Numerical Simulation for Optimization of the Experimental Setup. It was observed from our initial results that the attenuation values obtained from the experiments were generally much lower than in the reported literature.[13,22,32,33] After careful investigation, we observed that the experimental setups for determining attenuation were significantly different. Typically, the bistatic immersion configuration was used to estimate the acoustic properties in these experiments. The transducers were placed a few wavelengths away from the tested sample. The estimated attenuation of the signal included the reflection and dispersion effects. However, it is necessary to differentiate these effects from the energy loss in the signal since the attenuation effect is more composition-dependent than the fabrication process and microstructure-dependent to involve dispersion. In our proposed experimental setup, the transducer is in contact with the soft tissue samples or the tissue phantoms. It eliminates the effect of reflection, and the transmitted signal is affected solely due to the attenuation within the tissue. These numerical simulations reflect the difference in the acoustic wave propagation in our setup compared to that of other previous reports.

https://doi.org/10.1021/acsomega.2c06750
ACS Omega 2023, 8, 1319−1330

4.1.1. Reflection in the Conventional Bistatic Setup. Initially, numerical simulations were conducted based on the conventional bistatic experimental setup reported in the literature. This technique measures the acoustic transmission signal from the sample in water ambient. The sample was placed in water with the source and received transducers on the two sides, as illustrated in Figure 1. The transducers were usually kept apart from the sample by a distance longer than the operating wavelength. The measured acoustic properties are highly dependent on the alignment, sample surface conditions, and water conditions using this configuration.

Figure 3 shows the simulated pulse propagation in terms of acoustic pressure. Figure 3A–E on the left column represents

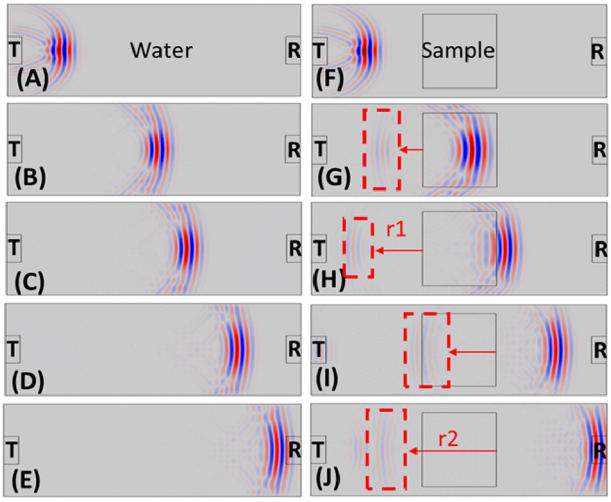

Figure 3. Pulse propagation simulation in terms of acoustic pressure using the suggested setup from the existing literature. (A–E) Reference measurement without the sample in the water ambient with the period of time for wave propagating from left to right. (F–J) Measurement with the sample placed in the water ambient with the period of time for wave propagating from left to right. In the subfigures, T refers to the emission source transducer. R indicates the receiver transducer port. In the red dash boxes, r1 and r2 were the reflection waves from the sample surfaces.

the pulse propagation with solely the transducer. Figure 3F–J on the right column depicts the pulse propagation through the gel without a finite attenuation. The experimental configuration on the left shows that the pulse propagation from the transducer is not affected by the surrounding media as there is no back reflection of the pulse. Figure 3G–J shows the back-reflected pulse from the gels indicated within the red-dashed block. For a transducer located a few wavelengths away from the gels, the energy loss by reflections (r1 and r2) may be incorrectly accounted for as attenuation. It can yield an incorrect inference of the acoustic loss or absorption in an ultrasonic imaging or tissue characterization modality. This extent of the reflection losses also depends on the difference in the elastic properties of the tissues with respect to the ambient water medium. When the sample properties are significantly different from water, the disparate sound speeds and the density difference will introduce significant uncertainties in the attenuation values from the conventional experimental setup reported in the literature.

Figure 4A shows the simulation result in terms of acoustic pressure for the monostatic experimental setup. Figure 4B illustrates the attenuation of a propagating wave within a

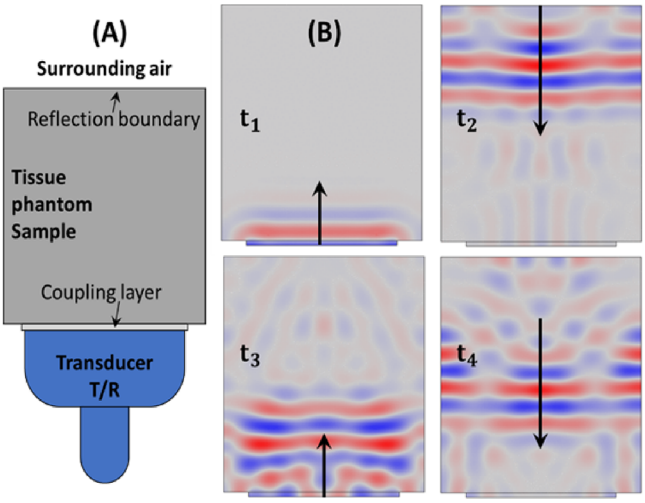

Figure 4. Simulation configuration and results for the acoustic property measurement setup with the transducer attached to gels. (A) Monostatic setup we suggested for the acoustic properties' measurement using the information of the first and second roundtrip reflections. (B) Numerical simulation results of the wave propagation behavior in terms of acoustic pressure from time t_1 to t_4.

medium that includes the first and second roundtrips. Close contact of the acoustic source with the tissue eliminates any loss due to multiple intermediate reflections. It ensures that all the energy loss is due to attenuation only in principle.

Figure 5A shows the simulation results from the bistatic immersion setup on two tissue phantoms with a slight difference. Gel 2 has a 5% higher speed of sound and density value than gel 1, and both gel 1 and gel 2 are considered non-dissipative without finite attenuation coefficients. Due to the higher speed of sound and density values on the gels, a higher transmission amplitude than water was expected. However, the result shows the energy loss due to the additional reflections. Although the attenuation coefficient is zero for both cases, the amplitude still shows a difference between the gels and the case without any sample. Moreover, due to the higher sound speed and density of gel 2, the larger impedance mismatching between gel 2 and water transferred more energy into the reflections. It results in a transmitted pulse intensity lower through gel 2 than in gel 1. Therefore, the energy loss from the impedance mismatch between ambient water and samples will also account for the attenuated signal in this configuration. The transmitted pulse ratio obtained from the signal through the gel (blue or red line) and the water ambient (black line) yields the gels' attenuation coefficient. The observed loss in the transmission signal amplitude is introduced in this measurement setup without the actual attenuation or dissipation within the sample. Therefore, the measured acoustic attenuation coefficient can be significantly overestimated with this bistatic experimental setup. The difference in the amplitude due to the energy loss will become even more pronounced as the difference in speed of sound and density value is further increased.

Figure 5B shows the result from the monostatic contact measurement method proposed in this study. The two pulses are reflected from the first and second roundtrips in the plot. The attenuation can be estimated from the ratio between those two pulses. On comparing the amplitude of the two echoes, only a negligible amount of energy loss due to the divergence of pulse can be observed in this case. Hence, in a practical case,

https://doi.org/10.1021/acsomega.2c06750
ACS Omega 2023, 8, 1319–1330

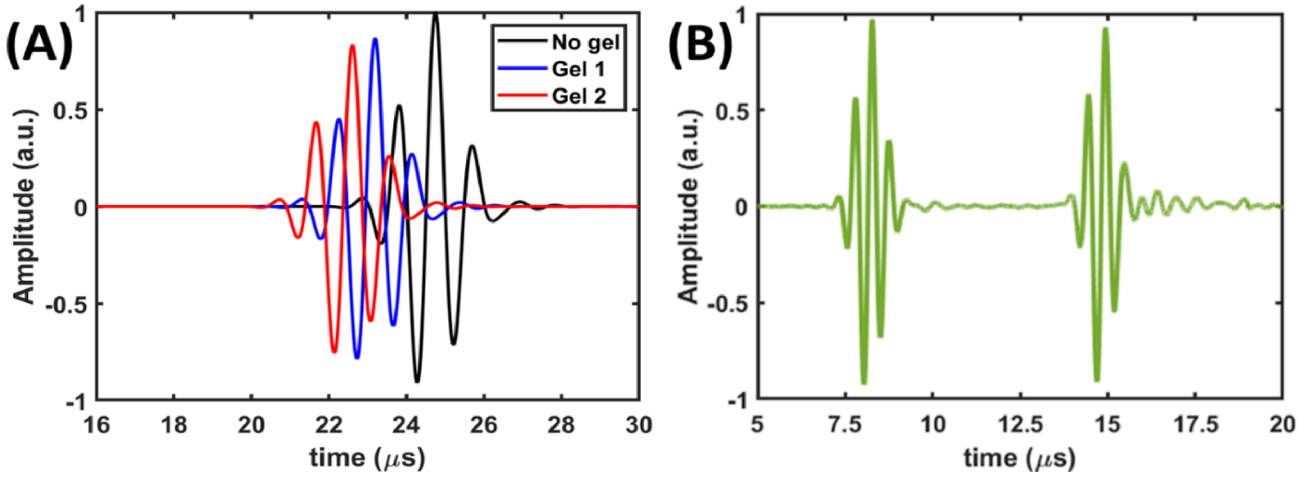

Figure 5. Comparison of temporal delay between two kinds of experimental setup. (A) Result from the bistatic immersion test, gel 1, and gel 2, in which gel 2 has a 5% higher speed of sound and density compared to gel 1. (B) Result for the monostatic contacting measurement methods.

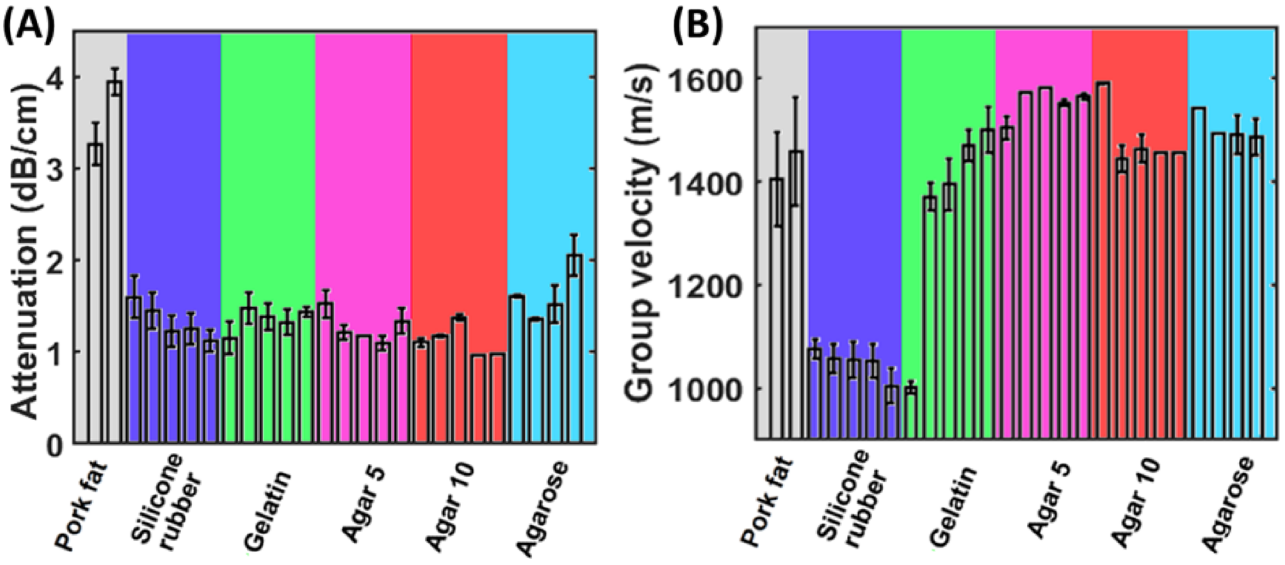

Figure 6. Summary of attenuation and speed of sound values for different kinds of tissue phantoms in this study using the conventional methods, which did not include any frequency dispersion effect. (A) Attenuation in dB/cm. (B) Group velocity in m/s. The properties in this figure estimated from the pulse envelope information. The horizontal axes indicate those conditions. The two bars in pork fat were the samples without and with skin. Five bars in silicone rubber referred to the different oil percentages from 10 to 50% with 10% intervals. Five bars in gelatin referred to the different milk percentages to replace water from 0 to 100% with a 25% interval. For the agar 5 and agar 10 samples, the five bars indicated the degassing process time from 0 to 4 min with 1 min intervals. The four bars in agarose samples referred to the degassing process time from 0 to 3 min with 1 min intervals.

it implies that the only significant contribution to the energy loss is due to the attenuation within the sample in this monostatic configuration compared to the additional loss from reflection with the conventional bistatic measurement configuration.

4.1.2. Dispersion. To account for the dispersion, a viscoelastic damping parameter is introduced in the simulation of gels with and without damping for the bistatic immersion configuration. Besides damping, the gel (without any attenuation) was assigned the identical sound velocity and density values as water to eliminate any reflection in this part of the study. In Figure 6A−C, we have depicted the acoustic pressure field for the acoustic wave propagating from the emission port to the receiver port. In Figure 6D, we can observe that the dispersive gel with damping has a significantly lower amplitude than the non-dispersive gel. The dispersion also results in an elongation of the temporal pulse width. This pulse broadening and the reduction of the peak pulse amplitude reduction due to dispersion may erroneously account for the attenuation within the medium.

Time-of-flight measurement is the most common way to measure the speed of sound value. The technique highly relies on seeking the peak amplitude of pulse envelopes. However, the dispersive nature of the medium results in a significant pulse shape distortion. From the point of view of energy dissipation, the dispersion effect does not directly dissipate the total acoustic energy of the pulse envelope. However, the out-of-phase component due to the dispersion reduces the peak amplitude of the source pulse and has commonly been considered as an attenuation. Comparisons found that the standard time-of-flight techniques underestimate the speed of sound by up to 10%, with variation in the frequency-dependent

https://doi.org/10.1021/acsomega.2c06750
ACS Omega 2023, 8, 1319−1330

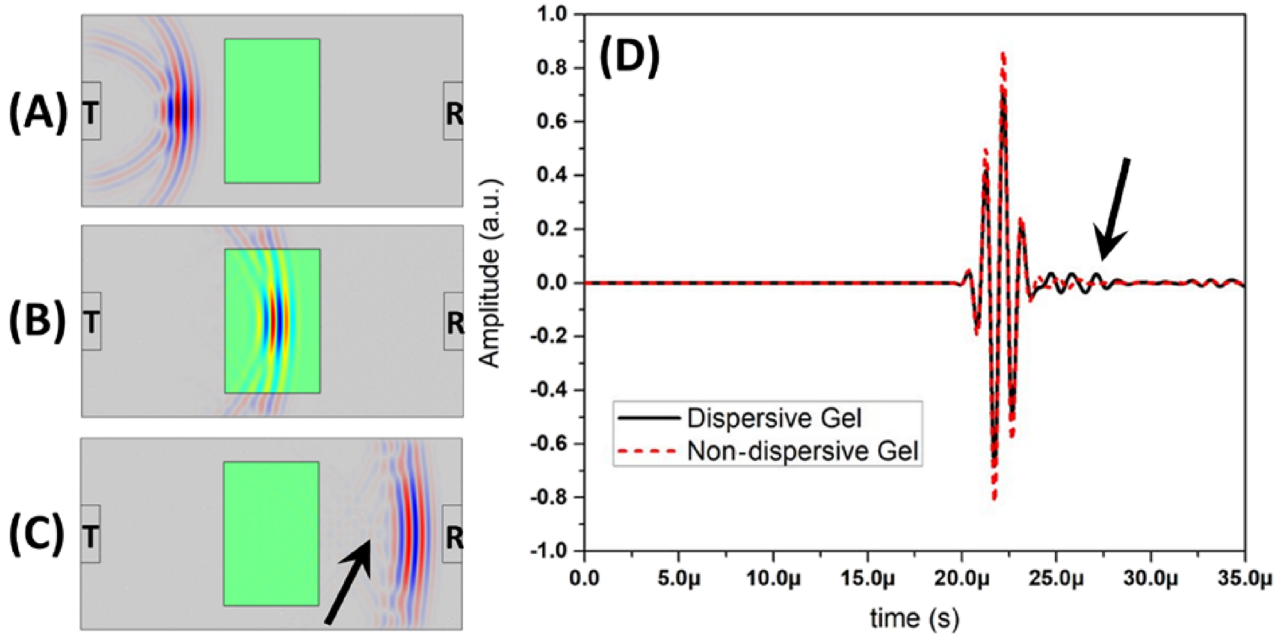

Figure 7. Dispersion contribution to energy dissipation. (A−C) Numerical simulation results of the acoustic pressure fields of the acoustic pulse propagating through a sample with the dispersion effect but a negligible attenuation effect. (D) Collected acoustic signal from the simulation (A−C), showing that the damping-induced dispersion decreased the received pulse amplitude by the out-of-phase effect.

speed of sound reaching as high as 200 m/s in the ultrasonic range of 0.2−0.8 MHz for bulk poly(vinyl alcohol) poly(*N*-isopropyl acrylamide) hydrogels.[34] The frequency dispersion further induced frequency-dependent dynamic elasticity in the hydrogels.[35] These findings can better characterize acoustic properties and higher resolution in ultrasonic imaging with dispersive media.

Acoustic pulse can accurately represent the dynamic elasticities of low dispersive or non-dispersive materials. Short pulses offer increased resolving power, especially in imaging or mapping mechanical properties, especially along the propagation direction. Short pulses feature a broadband frequency spectrum containing a wider range of frequency components. The relatively consistent behavior throughout a wide range of frequencies is centered at the fundamental pulse frequency. The fundamental frequency is well characterized in the analysis. For non-dispersive materials, the pulse's peak maxima are proportional to its fundamental frequency. However, frequency dispersion effects on the pulse envelope in a strong dispersive media can introduce inaccuracies into the traditional sound calculation speed as the time-of-flight measurements are exclusively assigned to a single frequency.

A significant difference between the actual time-of-flight and attenuation of the fundamental frequency can occur due to dispersion-induced out-of-phase effects. By correctly accounting for dispersive contributions, measurements that account for the frequency-dependent speed of sound can provide deeper insight into a material's mechanical properties. It is especially important in systems that use conventional approaches to assess the speed of sound and other mechanical properties using the center of a pulse envelope or the first detected peak for analysis. Inhomogeneous distribution of materials with different acoustic impedances and dispersions will strongly affect ultrasound imaging, especially for biomaterials. Analyzing the temporal elongation introduced in the pulse due to the dispersion in calculating the flight time and attenuation can provide deeper insight into the material, enhancing the depth and attenuation resolution caused by scattering or spatial inhomogeneity.

4.2. Experimental Measurements. Frequency (1 MHz) was initially used to operate with a long enough wavelength of the ultrasound to study the frequency-dependent attenuation and dispersion effect. Due to the existence of smaller air bubbles and internal layer structures in some of the tested samples, additional inhomogeneity can play a role in the tested medium with higher frequency. With a long enough operating wavelength for those internal structure sizes, the samples can still be considered homogeneous within the homogenization approximation limits used for the modeling. The additional impacts from the incoherent scattering can be properly minimized from the frequency-dependent attenuation and dispersion measurements.

The similarity between the tissue phantoms and natural fatty tissues was claimed in terms of the sound velocities and attenuation in the existing literature.[27] However, the tissue phantom and the porcine samples show drastically different attenuation when the reflection losses are eliminated. Figure 7A summarizes the attenuation and speed of sound values for all the tissue phantoms and porcine samples involved in this study. This figure shows that the natural porcine fat sample has a substantial attenuation (3.2−4 dB/cm) compared to the tissue phantoms (1−1.5 dB/cm). The agarose tissue phantom has a relatively high attenuation among all the tissue phantoms due to the neutral detergent. The significant difference in the group attenuation between the involved tissue phantoms and the natural fatty porcine samples was possibly due to the incomparable internal structures. The fatty porcine samples had more highly non-homogeneous internal structures than the relatively homogeneous mimicking tissue phantoms.[36,37] The additional energy loss in the fatty pork tissue due to internal scattering and back-scattering dissipates the transmitted acoustic pulses. The attenuation of sound waves in the tissue phantoms was increased by introducing the oil or milk into the phantom tissue recipes. The additional component in

https://doi.org/10.1021/acsomega.2c06750
ACS Omega 2023, 8, 1319−1330

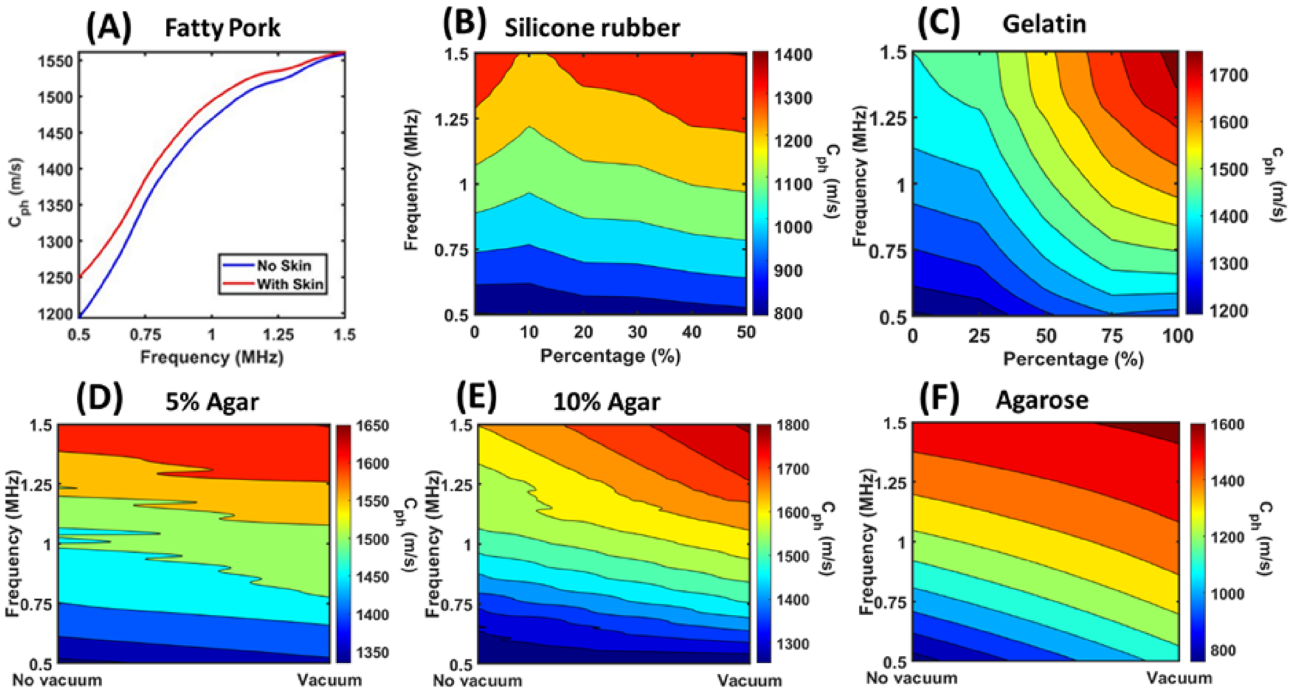

Figure 8. Dispersion summary for (A) pork fat with skin in the red line and pork fat without skin in the blue line (B). Silicone rubber with mineral oil varying from 0 to 50 wt % in 10 wt % intervals and (C) 10 wt % gelatin with evaporated milk varying from 0 to 100 wt % in 25 wt % intervals. (D−F) Frequency-dependent speed of sound contours of the 5% agar gels, 10% agar gels, and agarose tissue phantoms with and without vacuum processes.

the gel recipe increased the non-uniformity in the products, especially in the case of agar, agaroses, and silicone rubbers—the addition of oil-formed liquid−solid hybrid structures in the tissue phantoms. Part of the oil was stored in the phantoms as liquid pores but not well bonded, which enhanced the acoustic group attenuation values. The acoustic property of some tissue phantoms is time-dependent after being made due to dehydration and degradation. We performed acoustic monitoring on agar, gelatin, and silicone rubber posted in the Appendix section (Figure A1). Nevertheless, compared with the actual fatty pork samples, a significant difference still exists in acoustic attenuation. It means that if we want to use the mimic tissue to test the ultrasound imaging system or characterize the imaging signal, then increasing the thickness of the tissue phantom sample can be an alternative solution to compensate for the attenuation difference between the natural fatty tissue and tissue phantom.

Figure 7B compares the measured group velocity of sound in various materials. The overall trend is that silicone rubber has the lowest speed of sound value at around 1050 m/s. The 5 wt % agar gels have the highest speed of sound value at around 1550 m/s; other tissue phantoms have a similar speed of sound value, and it is comparable to the natural fatty tissue, which is around 1450 m/s. For the gelatin doped with evaporated milk, as the percentage of evaporated milk increased, the speed of sound value also increased from 1350 to 1500 m/s. For the silicone rubber mixed with mineral oil, as the mineral oil percentage increased, the speed of sound value decreased from 1090 to 1000 m/s. In comparison, we found that 10% agar gels, agarose gel, and milk gelatin have a speed of sound similar to the fatty porcine samples, around 1 MHz. The oil-filled silicone rubber shows the lowest sound velocity in this study. The tested results showed that the evaporated milk could increase sound speed, and mineral oil will reduce the speed of sound for tissue phantoms. Pork fat in room temperature and human fat at body temperature are different. However, both of the media can all be grouped into solid−liquid hybrid phase matrices together with high water-content hydrogel tissue phantoms. The temperature-dependent acoustic properties of those matrices would be very complex. Along with the ambient temperature increase, the solid matrices usually have decreasing speed of sound and increasing acoustic attenuation due to the increasing molecular distance. However, the liquid phase material in the matrices usually has increased sound speed and decreased acoustic attenuation due to the increasing molecular vibration. Further experimental measurement is necessary to determine the temperature-dependent acoustic properties.

Due to the strong viscoelastic nature of polymetric gel materials, the acoustic and mechanical properties are highly frequency-dependent. In the range of a longer operating wavelength with respect to the gels' microstructure, the gels show higher dynamic elasticity and speed of sound with higher operating frequency. The frequency-dependent speed of sound properties of pork fat, silicone rubber with mineral oil, and 10 wt % gelatin with evaporated milk are plotted in Figure 8. In Figure 8A, skinless pork fat has more significant dispersion than pork fat with skin. In Figure 8B, pure silicone rubber has the most extensive dispersion, and silicone rubber with 10 wt % mineral oil has the second largest dispersion. The dispersion values between 20 and 30 wt % mineral oil and between 40 and 50 wt % are very similar. The result suggests that mineral oil actually decreases the tissue phantom's dispersion. In Figure 8C, 10 wt % gelatin with 100 wt % evaporated milk exhibits the highest dispersion, while pure 10 wt % gelatin and 10 wt % gelatin with 25 wt % evaporated milk have similar and least dispersions, respectively. The result suggests that evaporated milk can increase the dispersion value of gelatin tissue

https://doi.org/10.1021/acsomega.2c06750
ACS Omega 2023, 8, 1319−1330

phantoms. In the agar-based gels, the air void commonly exists in the products due to the shorter curing time, which strongly deviates from the acoustic properties. Figure 8D−F compares the dispersion behaviors of 5 and 10% agar tissue phantoms and agarose tissue phantoms with and without the degassing process, respectively. The frequency-dependent sound velocity has an overall increase contributed by the vacuum process in all three tissue phantoms due to reducing the air volume fraction. From the contours, we observed that the frequency dispersion effect was not uniform in the agar tissue phantoms without the degassing process. This non-uniformity can be caused by large voids comparable to the size of the wavelength. After the vacuum process, the uniformity in the frequency dependence of the sound velocity of the 10% agar tissue phantom is enhanced. In the 5% agar tissue phantom samples, the phase velocity referred to the decreasing void volume fraction but still with a size comparable to the operating wavelength. From the phase velocity maps, the observation clearly showed that the acoustic dispersion effect in the tissue phantoms was highly dependent on the composition ratio and fabrication processes that have barely been pointed out in the existing literature. To properly determine the dispersive sound velocity in natural tissue and tissue phantoms is a necessary procedure for accurate development or training on biomedical ultrasound imaging.

Figure 9A shows the attenuation value for tissue phantoms in dB/mm. Attenuation of ultrasound waves is generated by reflections, divergence, scattering from inhomogeneities, and dissipation. Among these factors, dissipation is the most significant source of attenuation in diagnostic ultrasound. Higher frequency waves are attenuated more quickly than lower frequency waves and yield smaller penetration depths for imaging applications. There is a trade-off between higher resolution at a higher frequency and deeper penetration depths at a lower frequency. This figure indicates that the porcine fatty tissue has the highest attenuation, which indicates that higher frequency ultrasound will not have deep penetration in this medium. Figure 9B summarizes the normalized dispersion properties of the tissue phantoms. The normalized dispersion was estimated by subtracting the frequency-dependent speed of sound function from the speed of sound at the lowest frequency component within the bandwidth under investigation. In this plot, we can see that 10 wt % agar gels have the highest dispersion, and 5 wt % agar gels, on the other hand, have the lowest dispersion value. Gelatin gels with evaporated milk have the closest dispersion value compared to port fatty tissues, which means that gelatin is a potential candidate for mimicking fatty tissue phantoms in terms of dispersion value. As stated before, the dispersion value can affect the temporal resolution by elongating the pulse width; proper dispersion characterization is vital for ultrasound imaging.

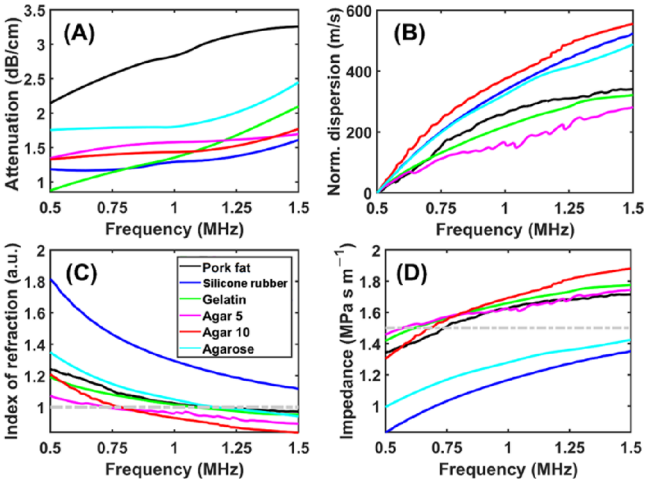

Figure 9. Summary of the frequency-dependent acoustic properties of all the tissue phantoms involved in this study. (A) Attenuation, (B) normalized dispersion, (C) index of refraction, and (D) acoustic impedance.

In Figure 9C,D, the gray lines indicate the property of water. In Figure 9C, acoustic impedances were calculated using the equation $z = \rho c$ for plane wave, where ρ is the density of tissue phantoms and c is the speed of sound of tissue phantoms. As shown in Figure 9C, the impedance value of water at room temperature is around 1.5 MPa·s·m^{-1}. Due to the lowest speed of sound of the silicone rubber compared to other tissue phantoms, silicone rubber has the lowest impedance value. Agarose has an average density of less than 890 kg/m^3, which is the lowest among all the samples. Therefore, agarose also has a relatively low impedance value. The rather large contrast of the impedance value between silicone rubber, agarose, and water in the frequency range from 0.5 to 1.5 MHz will provide a clear signal. However, for pork fat, gelatin, 5 wt % agar, and 10 wt % agar, there is an intercept with water in the frequency range of 0.5−0.75 MHz. There will be a cloaking effect around the intercept frequency range, which means that the similar impedance value fails to provide a clear signal during ultrasound transmission and blur imaging. Figure 9D shows the plot of the index of refraction. The change in direction when ultrasound waves are transmitted into another medium is refraction, an essential characteristic in some clinical imaging applications. The value of the index of refraction for water at room temperature is 1. Other than silicone rubber, all the other tissue phantoms have an intercept of the index of refraction with water, and the imaging will get distorted around the intercept region.

4.3. Demonstrating Clarity Enhancement by Including Attenuation and Dispersion Corrections. The above additional acoustic characterizations can combine with post-processing techniques and enhance the resolution of ultrasound imaging in a lab environment at the current stage. For a proof of concept, we collected a set of the raster-scanned ultrasound imaging data of gelatin-sealed biomasses (Figure 10A) with the experimental configuration shown in subfigure B. The four samples were categorized into a homogenized artificial material (gum), biomass with relative uniform elasticity (green bean), biomass with a smooth, hard skin (corn), and biomass with a rough hard skin (dry grape). The echo-intensity and time-of-flight information were collected from the temporal data set, which were constructed into the echo-intensity image and time-of-flight image in subfigures C and D, respectively. The normalized echo-intensity and time-of-flight images were posted in subfigures E and F, respectively. Based on the pre-characterization, the acoustic dispersion and attenuation effects were weakened by the frequency domain normalization of the phase delay and absolute amplitude in the 10% gelatin tissue phantom. Inverse Fourier transformation converted the normalized frequency domain data back into the temporal domain. The normalized frequency domain data was converted back into the temporal domain by inverse Fourier transformation.

https://doi.org/10.1021/acsomega.2c06750
ACS Omega 2023, 8, 1319−1330

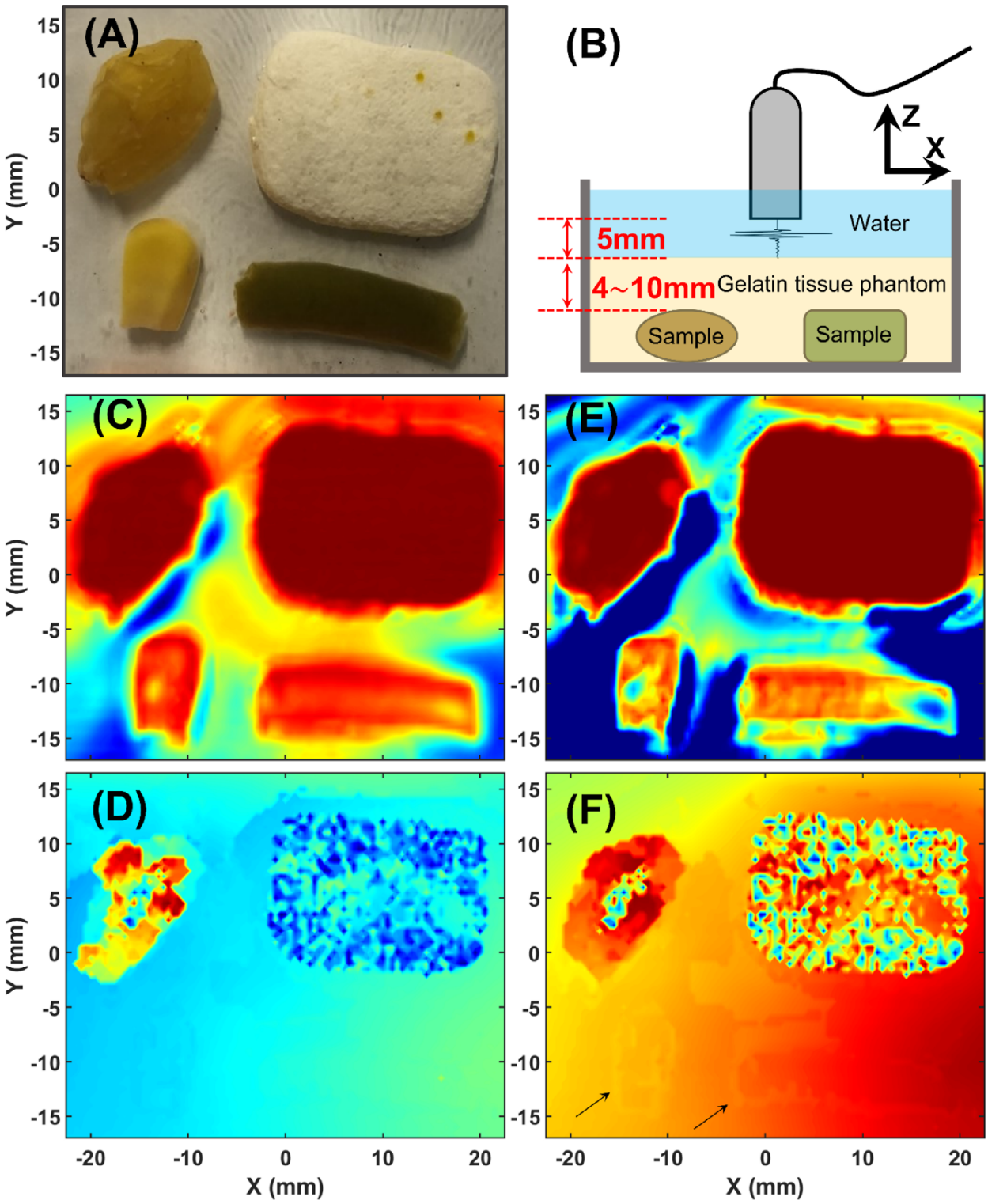

Figure 10. Raster scan constructed ultrasound images of dry grape, gum, corn, and green bean in a 10% gelatin tissue phantom. (A) Photograph of the sample. (B) Illustration of the side view of the scan configuration. (C) Raw echointensity imaging. (D) Raw time-of-flight imaging. (E) Dispersion and attenuation normalized echo-intensity imaging. (F) Dispersion and attenuation normalized time-of-flight imaging.

From subfigures A and C to F, the clarity enhancement in echo-intensity images (from C to E) was significant. The attenuation and dispersion effect normalization provided more distinguishable contrast gelatin background and imaged targets. The sizes of the objects became more comparable to the photograph. The dispersion correction weakened the gelatin curing and induced residual stress between the biomasses.[38] From the contribution of the shear modulus of gelatin tissue phantoms, the harder biomasses surrounded by gelatin have an effectively higher deformation resistance at the gelatin side around the sample/gelatin interface, which blurs the target boundaries of biomasses. The elimination of the dispersion effect in gelatin further cleared the sample-background boundaries in the echo-intensity image, especially

https://doi.org/10.1021/acsomega.2c06750
ACS Omega 2023, 8, 1319−1330

around corn and green bean. Compared with the time-of-flight images (subfigures D and F), the post-processing highlighted the shape of the dry grape due to the elimination of the pulse dispersion from the high roughness dry grape reflection surface. Furthermore, in the lower region ($Y = -5$ to -15 mm) of the time-of-flight images, the corn and green bean were cloaked in the raw time-of-flight image. However, after the normalization of attenuation and dispersion effects, in the processed image (subfigure F), we can see two shadows located at the corn and green bean positions with approximately correct shapes. The presence of the two shadows was contributed by the boundaries between gelatin and corn/bean in the processed image due to the correction of sound-velocity-mismatching induced pulse dispersion. In general, the results showed an apparent enhancement in the clarity of the ultrasound images, such as the conventional A or B mode-like imaging configurations. For practical applications, more studies need to be conducted, such as pre-characterization of attenuation and dispersion effects on the real fatty tissues and soft tissues, system integrations, and developments of the longitude-wave-based imaging system.

5. CONCLUSIONS

In this work, we have studied the acoustic properties and the corresponding experimental methods of some fatty tissue phantoms made by the commonly used recipes in the literature. First, we have conducted a numerical simulation of acoustic wave time of flight on the conventional acoustic property testing method. We found that the acoustic attenuation values from the in-water bistatic methods included additional energy loss and uncertainties such as reflections and dispersion. The additional energy loss and the uncertainties increased measured attenuation values from the technique. The in-air monostatic methods we suggested from the simulation decreased additional energy loss significantly; therefore, the tested values are closer to actual attenuation values. Another way to avoid overestimating the attenuation values for the in-water bistatic experiment is to move the sample closer to the transducer and detector to ensure that the distance between the sample, transducer, and detector is less than 1/4 of the operating wavelength to achieve maximum transmissivity. Second, we have characterized attenuation and frequency dispersion in some commonly used fatty tissue phantoms, which were barely discussed in the existing literature. Including acoustic dispersion, frequency-dependent sound velocity, and attenuation, the similarities of the fatty tissue phantoms and the fatty porcine samples were compared with each other. The results concluded that the involved fatty tissue phantoms offered comparable group velocity and frequency dispersion around 1 MHz operating frequency. Nevertheless, the fatty porcine sample's acoustic attenuation still exceeded the tissue phantoms' range in terms of pulse envelope and its frequency components. These additional acoustic characterizations can combine with post-processing techniques and enhance the resolution of ultrasound imaging in a lab environment at the current stage. Last, we performed a proof-of-concept ultrasound imaging experiment with one of the characterized fatty tissue phantoms and some biomasses. By weakening the attenuation and dispersion effects via signal processing, the quality of the ultrasound images was clearly improved.

APPENDIX

The acoustic monitoring on agar, gelatin, and silicone rubber posted is shown in Figure A1.

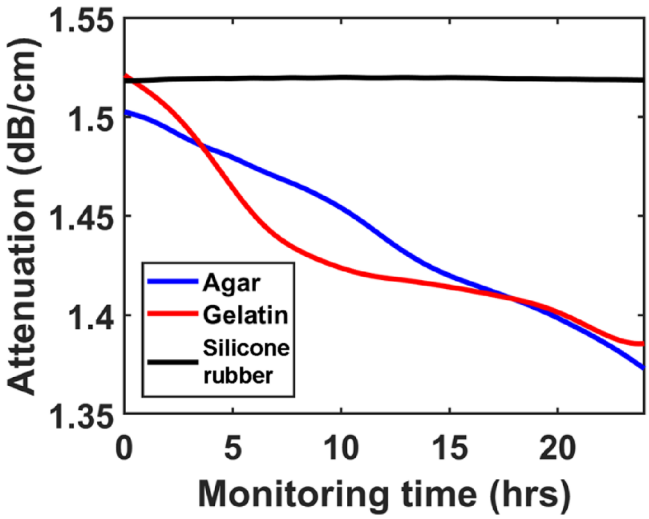

Figure A1. Longitudinal data (time-dependent monitoring) on agar, gelatin, and silicone rubber tissue phantoms in 24 h under ventilating air ambient at 30% relative humanity and a 22 °C environment.

AUTHOR INFORMATION

Corresponding Author

Arup Neogi − *Department of Physics, University of North Texas, Denton, Texas 76203, United States; Institute of Fundamental and Frontier Sciences, University of Electronic Science and Technology of China, Chengdu 611731, P. R. China*; Email: arup@uestc.edu.cn

Authors

Teng Yang − *Department of Physics, University of North Texas, Denton, Texas 76203, United States; Department of Materials Science and Engineering, University of North Texas, Denton, Texas 76207, United States*

Yuqi Jin − *Department of Physics, University of North Texas, Denton, Texas 76203, United States;* orcid.org/0000-0001-7798-8086

Complete contact information is available at: https://pubs.acs.org/10.1021/acsomega.2c06750

Notes

The authors declare no competing financial interest.

ACKNOWLEDGMENTS

This work is supported by the Ministry of Science and Technology of China (MOST) International Collaboration grant #2022YFE0129000 entitled "Cavity Acoustodynamics for Nonreciprocal Wave Propagation". A.N. also acknowledges the support from the Distinguished Professorship start-up funds from UESTC.

REFERENCES

(1) Newman, M. E., *Soft Tissue Sarcomas: Current and Emerging Trends in Detection and Treatment*; The Rosen Publishing Group, Inc: 2011.

(2) Sandusky, G. E.; Teheny, K. H.; Esterman, M.; Hanson, J.; Williams, S. D. Quality control of human tissues-experience from the

Indiana University Cancer Center-Lilly Research Labs human tissue bank. *Cell Tissue Banking* **2007**, *8*, 287−295.
(3) Khov, N.; Sharma, A.; Riley, T. R. Bedside ultrasound in the diagnosis of nonalcoholic fatty liver disease. *World J. Gastroenterol.* **2014**, *20*, 6821.
(4) Bril, F.; Ortiz-Lopez, C.; Lomonaco, R.; Orsak, B.; Freckleton, M.; Chintapalli, K.; Hardies, J.; Lai, S.; Solano, F.; Tio, F.; Cusi, K. Clinical value of liver ultrasound for the diagnosis of nonalcoholic fatty liver disease in overweight and obese patients. *Liver Int.* **2015**, *35*, 2139−2146.
(5) Cohen, E. B.; Afdhal, N. H. Ultrasound-based hepatic elastography: origins, limitations, and applications. *J. Clin. Gastroenterol.* **2010**, *44*, 637−645.
(6) Palma-Chavez, J.; Wear, K. A.; Mantri, Y.; Jokerst, J. V.; Vogt, W. C. Photoacoustic imaging phantoms for assessment of object detectability and boundary buildup artifacts. *Photoacoustics* **2022**, *26*, No. 100348.
(7) Palma-Chavez, J.; Pfefer, T. J.; Agrawal, A.; Jokerst, J. V.; Vogt, W. C. Review of consensus test methods in medical imaging and current practices in photoacoustic image quality assessment. *J. Biomed. Opt.* **2021**, *26*, No. 090901.
(8) Pehrson, L. M.; Lauridsen, C.; Nielsen, M. B. Machine learning and deep learning applied in ultrasound. *UiM/EJU* **2018**, *39*, 379−381.
(9) Wu, T.; Sultan, L. R.; Tian, J.; Cary, T. W.; Sehgal, C. M. Machine learning for diagnostic ultrasound of triple-negative breast cancer. *Breast Cancer Res. Treat.* **2019**, *173*, 365−373.
(10) Kainz, B.; Heinrich, M. P.; Makropoulos, A.; Oppenheimer, J.; Mandegaran, R.; Sankar, S.; Deane, C.; Mischkewitz, S.; al-Noor, F.; Rawdin, A. C.; Ruttloff, A.; Stevenson, M. D.; Klein-Weigel, P.; Curry, N. Non-invasive diagnosis of deep vein thrombosis from ultrasound imaging with machine learning. *NPJ Digit. Med.* **2021**, *4*, 137−118.
(11) Rana, S. P.; Dey, M.; Tiberi, G.; Sani, L.; Vispa, A.; Raspa, G.; Duranti, M.; Ghavami, M.; Dudley, S. Machine learning approaches for automated lesion detection in microwave breast imaging clinical data. *Sci. Rep.* **2019**, *9*, 10510.
(12) Jones, R. M. Tissue Substitutes, Phantoms and Computational Modelling in Medical Ultrasound-ICRU Report 61. *Health Phys.* **2000**, *78*, 344−344.
(13) Cafarelli, A.; Verbeni, A.; Poliziani, A.; Dario, P.; Menciassi, A.; Ricotti, L. Tuning acoustic and mechanical properties of materials for ultrasound phantoms and smart substrates for cell cultures. *Acta Biomater.* **2017**, *49*, 368−378.
(14) Menikou, G.; Damianou, C. Acoustic and thermal characterization of agar based phantoms used for evaluating focused ultrasound exposures. *J. Ther. Ultrasound* **2017**, *5*, 14.
(15) Cook, J. R.; Bouchard, R. R.; Emelianov, S. Y. Tissue-mimicking phantoms for photoacoustic and ultrasonic imaging. *Biomed. Opt. Express* **2011**, *2*, 3193−3206.
(16) Nguyen, M. M.; Zhou, S.; Robert, J. L.; Shamdasani, V.; Xie, H. Development of oil-in-gelatin phantoms for viscoelasticity measurement in ultrasound shear wave elastography. *Ultrasound Med. Biol.* **2014**, *40*, 168−176.
(17) Zarrintaj, P.; Manouchehri, S.; Ahmadi, Z.; Saeb, M. R.; Urbanska, A. M.; Kaplan, D. L.; Mozafari, M. Agarose-based biomaterials for tissue engineering. *Carbohydr. Polym.* **2018**, *187*, 66−84.
(18) Aranda-Lara, L.; Torres-García, E.; Oros-Pantoja, R. Biological tissue modeling with agar gel phantom for radiation dosimetry of ^{99m}Tc. *Open J. Radiol.* **2014**, *04*, 44−52.
(19) Wear, K. A. The Effects of Frequency-Dependent Attenuation and Dispersion on Sound Speed Measurements: Applications in Human Trabecular Bone. *IEEE Trans. Ultrason. Ferroelectr. Freq. Control* **2000**, *47*, 265−273.
(20) Daniels, A. U. Silicone breast implant materials. *Swiss Med. Wkly.* **2012**, 29.
(21) Ustbas, B.; Kilic, D.; Bozkurt, A.; Aribal, M. E.; Akbulut, O. Silicone-based composite materials simulate breast tissue to be used as ultrasonography training phantoms. *Ultrasonics* **2018**, *88*, 9−15.
(22) Farrer, A. I.; Odéen, H.; de Bever, J.; Coats, B.; Parker, D. L.; Payne, A.; Christensen, D. A. Characterization and evaluation of tissue-mimicking gelatin phantoms for use with MRgFUS. *J. Ther. Ultrasound* **2015**, *3*, 1−11.
(23) Wang, Y.; Tai, B. L.; Yu, H.; Shih, A. J., Silicone-based tissue-mimicking phantom for needle insertion simulation. *J. Med. Device.***2014**, *8* (), DOI: 10.1115/1.4026508.
(24) Langer, R.; Tirrell, D. A. Designing materials for biology and medicine. *Nature* **2004**, *428*, 487−492.
(25) Madsen, E. L.; Frank, G. R.; Dong, F. Liquid or solid ultrasonically tissue-mimicking materials with very low scatter. *Ultrasound Med. Biol.* **1998**, *24*, 535−542.
(26) Svec, F.; Tennikova, T. B.; Deyl, Z.*Monolithic materials: preparation, properties and applications*; Elsevier: 2003.
(27) Ortega, R.; Leija, L.; Vera, A., Measurement of ultrasonic properties of fat biological phantom. In *2009 Pan American Health Care Exchanges*; IEEE2009, *58*−61.
(28) Hikage, T.; Sakaguchi, Y.; Nojima, T.; Koyamashita, Y., Development of lightweight solid phantom composed of silicone rubber and carbon nanotubes. In *2007 IEEE International Symposium on Electromagnetic Compatibility*; IEEE2007, 1−4.
(29) Sindi, R.; Wong, Y. H.; Yeong, C. H.; Sun, Z. Development of patient-specific 3D-printed breast phantom using silicone and peanut oils for magnetic resonance imaging. *Quant. Imaging. Med. Surg.* **2020**, *10*, 1237.
(30) Matthew, O. D.; Jaynes, E. T.; Miller, J. G. Kramers−Kronig relationship between ultrasonic attenuation and phase velocity. *J. Acoust. Soc. Am.* **1981**, *69*, 696−701.
(31) Strelitzki, R.; A, E. J. On the measurement of the velocity of ultrasound in the os calcis using short pulses. *Eur. J. Ultrasound* **1996**, *4*, 205−213.
(32) Amidi, E.; Yang, G.; Uddin, K. S.; Wahidi, R.; Zhu, Q., Low-cost ultrasound and optical gelatin-based phantoms. *InPhotons Plus Ultrasound: Imaging and Sensing*; SPIE2019, *10878*, 108784A.
(33) Józefczak, A.; Kaczmarek, K.; Kubovčíková, M.; Rozynek, Z.; Hornowski, T. The effect of magnetic nanoparticles on the acoustic properties of tissue-mimicking agar-gel phantoms. *J. Magn. Magn. Mater.* **2017**, *431*, 172−175.
(34) Jin, Y.; Heo, H.; Walker, E.; Krokhin, A.; Choi, T. Y.; Neogi, A. The effects of temperature and frequency dispersion on sound speed in bulk poly (Vinyl Alcohol) poly (N-isopropylacrylamide) hydrogels caused by the phase transition. *Ultrasonics* **2020**, *104*, 105931.
(35) Jin, Y.; Yang, T.; Ju, S.; Zhang, H.; Choi, T.-Y.; Neogi, A. Thermally Tunable Dynamic and Static Elastic Properties of Hydrogel Due to Volumetric Phase Transition. *Polymer* **2020**, *12*, 1462.
(36) Jiang, Y.; Joanna, L.-H. Y.; Lee, J. H.; An, J.; Steadman, P. E.; Kim, J.-R.; Sung, H.-K. Visualization of 3D white adipose tissue structure using whole-mount staining. *JoVE* **2018**, *141*, No. e58683.
(37) Galic, S.; Oakhill, J. S.; Steinberg, G. R. Adipose tissue as an endocrine organ. *Mol. Cell. Endocrinol.* **2010**, *316*, 129−139.
(38) Drescher-Krasicka, E.; Willis, J. R. Mapping stress with ultrasound. *Nature* **1996**, *384*, 52−55.